Published in final edited form as:

Mol Pharm. 2023 August 07; 20(8): 4285–4296. doi:10.1021/acs.molpharmaceut.3c00390.

Process Robustness in Lipid Nanoparticle Production: A Comparison of Microfluidic and Turbulent Jet Mixing

Matthew N. O'Brien Laramy,
Genentech, Inc., Genentech Research and Early Development, Synthetic Molecule Pharmaceutical Sciences, South San Francisco, California 94060, United States

Antonio P. Costa,
DIANT Pharma, Inc., Manchester, Connecticut 06042, United States

Yareli Maciel Cebrero,
Genentech, Inc., Genentech Research and Early Development, Synthetic Molecule Pharmaceutical Sciences, South San Francisco, California 94060, United States

Johnson Joseph,
DIANT Pharma, Inc., Manchester, Connecticut 06042, United States

Apoorva Sarode,
Genentech, Inc., Genentech Research and Early Development, Synthetic Molecule Pharmaceutical Sciences, South San Francisco, California 94060, United States

Nanzhi Zang,
Genentech, Inc., Genentech Research and Early Development, Synthetic Molecule Pharmaceutical Sciences, South San Francisco, California 94060, United States

Lee Joon Kim,
Lawrence Berkeley National Laboratory, Molecular Biophysics and Integrated Bioimaging Division, Berkeley, California 94720, United States

Kate Hofmann,
Genentech, Inc., Genentech Research and Early Development, Synthetic Molecule Pharmaceutical Sciences, South San Francisco, California 94060, United States

Shirley Wang,
Genentech, Inc., Genentech Research and Early Development, Synthetic Molecule Pharmaceutical Sciences, South San Francisco, California 94060, United States

Alexandre Goyon,

Corresponding Authors Matthew N. O'Brien Laramy – obrienlm@gene.com; **Antonio P. Costa** – costa@diantpharma.com.

ASSOCIATED CONTENT

Supporting Information

The Supporting Information is available free of charge at https://pubs.acs.org/doi/10.1021/acs.molpharmaceut.3c00390.
DLS and %E data is provided for each LNP sample produced; lipid composition data for ASO-LNPs produced with the coaxial turbulent jet mixer; qualitative and quantitative description of the CryoEM data; statistical modeling data for the ASO-LNPs generated with each mixer; SAXS data are shown for each sample; additional CryoEM images are shown for each sample shown in the main text; additional comparison of sample data for LNPs produced by each mixer (PDF)

The authors declare the following competing financial interest(s): M.N.O.L., A.S., N.Z., A.G., and S.G.K. are employees of Genentech, Inc. A.P.C. and J.J. are employees of DIANT Pharma, Inc.

Genentech, Inc., Genentech Research and Early Development, Synthetic Molecule Pharmaceutical Sciences, South San Francisco, California 94060, United States

Stefan G. Koenig,
Genentech, Inc., Genentech Research and Early Development, Synthetic Molecule Pharmaceutical Sciences, South San Francisco, California 94060, United States

Michal Hammel,
Lawrence Berkeley National Laboratory, Molecular Biophysics and Integrated Bioimaging Division, Berkeley, California 94720, United States

Greg L. Hura
Lawrence Berkeley National Laboratory, Molecular Biophysics and Integrated Bioimaging Division, Berkeley, California 94720, United States; University of California Santa Cruz, Department of Chemistry and Biochemistry, Santa Cruz, California 95064, United States

Abstract

The recent clinical and commercial success of lipid nanoparticles (LNPs) for nucleic acid delivery has incentivized the development of new technologies to manufacture LNPs. As new technologies emerge, researchers must determine which technologies to assess and how to perform comparative evaluations. In this article, we use a quality-by-design approach to systematically investigate how the mixer technology used to form LNPs influences LNPstructure. Specifically, a coaxial turbulent jet mixer and a staggered herringbone microfluidic mixer were systematically compared via matched formulation and process conditions. A full-factorial design-of-experiments study with three factors and three levels was executed for each mixer to compare process robustness in the production of antisense oligonucleotide (ASO) LNPs. ASO-LNPs generated with the coaxial turbulent jet mixer were consistently smaller, had a narrower particle size distribution, and had a higher ASO encapsulation as compared to the microfluidic mixer, but had a greater variation in internal structure with less ordered cores. A subset of the study was replicated for mRNA-LNPs with comparable trends in particle size and encapsulation, but more frequent bleb features for LNPs produced by the coaxial turbulent jet mixer. The study design used here provides a road map for how researchers may compare different mixer technologies (or process changes more broadly) and how such studies can inform process robustness and manufacturing control strategies.

Graphical Abstract

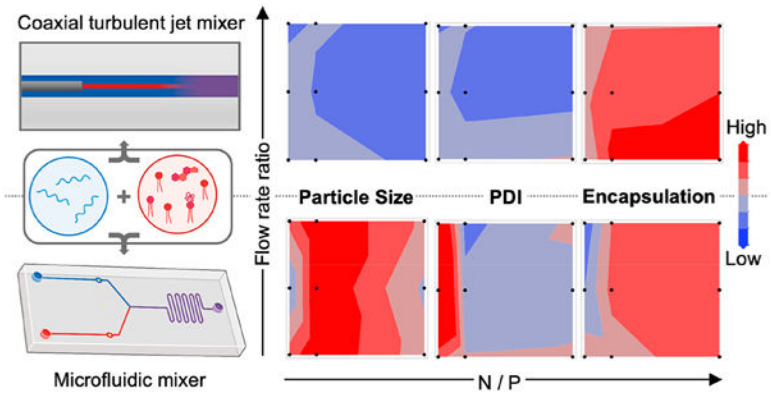

Keywords

lipid nanoparticle; nucleic acid; antisense oligonucleotide; messenger RNA; turbulent jet mixer; microfluidic mixer

1. INTRODUCTION

Lipid nanoparticles (LNPs) are the most clinically successful class of drug delivery vehicles for nucleic acids.[1–6] LNP formulations can be designed to encapsulate and protect nucleic acids from degradation, to modulate pharmacokinetics and biodistribution, to enhance cellular uptake and intra-cellular activity, and to stimulate immune responses. Each of these functional properties can be modulated by the nucleic acid design, the lipid composition, other formulation components, and the manufacturing process.[7–12]

LNPs typically include four classes of lipids: phospholipids, sterols, ionizable lipids, and lipopolymers.[13] Each lipid class confers unique attributes to the LNP, but also acts in a synergistic fashion with other lipids, the nucleic acid(s), and the surrounding environment to modulate the LNP structure. Phospholipids and sterols are hypothesized to act as "structural" lipids that enclose and stabilize the LNP, with additional lipid in the interior.[14,15] Ionizable lipids typically have branched fatty acid tails and an ionizable headgroup. This structure enables the lipid to complex with negatively charged nucleic acid backbones at acidic pH (i.e., below the pK_a of the ionizable headgroup) and thus encapsulate the nucleic acid in the interior of the LNP.[16,17] Lipopolymers are hypothesized to control the size and size distribution during LNP formation and typically reside in the outer surface of the LNP to confer colloidal stability. Each of these lipids has further functions to influence the biological activity in vitro and in vivo.

LNP manufacturing is typically performed in a series of discrete unit operations, including the following: dissolving lipids in an organic solvent (e.g., ethanol), dissolving nucleic acid(s) in an acidic aqueous solution, mixing of the organic and aqueous solutions to form the LNP, solution exchange to remove ethanol and replace it with a storage solution near physiological pH, concentration, and sterile filtration.[1,14,18] If mixing is slow or incomplete during the LNP formation step, then this may result in a larger nanoparticle size, broader particle size distribution, and decreased nucleic acid encapsulation.[18,19] Consequently, the rate and manner of mixing are critical to the formation of uniform LNPs with controlled physicochemical properties and structure. The presence of residual ethanol and changes in the pH, ionic content, and osmolality of the surrounding environment can further modulate LNP physicochemical properties and structure.[11]

Within published research, passive microfluidic mixing is the most studied technique to produce LNPs.[18,20–22] Passive microfluidic mixers use fluid flow through microchannels to introduce and mix two solutions under laminar flow conditions with a low Reynolds number (*Re*, where $Re \ll 100$).[23] Under laminar flow, mixing of solutions primarily occurs via diffusion (i.e., across a concentration gradient), and when mixed at the microfluidic length scale, the diffusion length (and thus the mixing time) is reduced compared to bulk mixing. Obstructions can be designed into microfluidic pathways to generate transverse

flow components that increase the contact area between fluids and reduce diffusion length through a process called chaotic advection.[19,23,24] If the characteristic diffusion length is reduced, then the faster mixing that results can enable smaller LNP size and greater encapsulation of nucleic acids in the LNP (%E; i.e., the fraction of nucleic acid that is encapsulated in the LNP).[19,24] A reduction in the characteristic diffusion length can be accomplished through modification of the mixer geometry, an increase in the total flow rate (TFR; i.e., the combined flow rate of the aqueous and organic solutions), or an increase in the flow rate ratio (FRR; i.e., the relative flow rate of the aqueous solution to the organic solution).

Two of the most studied passive microfluidic mixer geometries in research are the staggered herringbone mixer (SHM; Classic cartridge) and the bifurcated toroidal mixer (NxGen cartridge) commercialized by Precision Nanosystems, Inc.[18,19,21,24–26] These mixers are frequently used due to the commercial availability of the technology, the ability to use small quantities of material per experiment (<0.5 mL), the minimal operator intervention required, and the ability to achieve rapid mixing that yields uniform LNPs. Process scale-up can be achieved through parallelization of the microfluidic chambers, longer flow duration, or careful redesign of the mixer geometry to enable comparable mixing at higher flow rates.[18,21,26,27] Potential limitations associated with microfluidic mixing approaches include environmental waste and cost associated with single-use disposable cartridges, cartridge-to-cartridge variability, and incompatibility of the cartridge materials with certain solvents. However, it is worth noting that commercially available cartridges are compatible with ethanol, the most used organic solvent, and that variation between cartridges typically results in minimal differences in LNP quality attributes. Commercial offerings are currently sold as stand-alone equipment that may not be easily integrated into a continuous process paradigm or adapted to include in-process analytics.

By contrast, turbulent jet mixers operate at a higher Reynolds number (e.g., $100 < Re < 2000$) and rely on inertial forces to generate random fluid motion that enables convective mass transport in all directions. Under these mixing conditions, the interfacial area between two solutions is increased, such that mixing occurs rapidly. To generate turbulent conditions, two solutions can be injected into each other at high velocity (i.e., as one or more jets), either in the same or opposite direction. If injected in coflow (i.e., the same direction), then a jet can form that is characterized by a regime of limited mixing, followed by a confined turbulent zone where mixing occurs rapidly. When applied to nanoparticle formation, the size and size distribution of the nanoparticles are dependent on the Reynold's number of the turbulent mixing region, in addition to other process parameters and material attributes.[28,29]

A coaxial turbulent jet in coflow mixer technology (i.e., the DIANT jet) was recently developed as part of a continuous manufacturing platform at the University of Connecticut and commercialized by DIANT Pharma, Inc.[29–32] The DIANT jet is composed of two concentric tubes, where an organic solution is injected in the same flow direction as an aqueous solution to form a jet. Process scale-up can be achieved without parallelization through modification of the mixer design, increased flow rate, and a longer flow duration. This coaxial turbulent jet mixing technology does not use disposable mixing chambers, has broad solvent compatibility due to stainless-steel construction, and lacks micrometer-scale

features that may become clogged. In addition, the commercial offerings of the mixing technology can have integrated in-process controls and analytics for temperature, flow rate, and particle size, and can be integrated into a continuous manufacturing process with tangential flow filtration and sterile filtration units. While this mixing technology has been successfully used to produce uniform liposomes and polymeric nanoparticles,[29–32] LNP production has not been previously reported with this technology. Potential limitations associated with this mixer technology are the larger volumes required for each experiment (typically >20 mL), the need to clean the mixing chamber between each run, and the nascent state of technology (and continuous manufacturing technology in the pharmaceutical industry, more generally).

In this article, a quality-by-design approach[24,32,33] was used to compare LNP formation via microfluidic and coaxial turbulent jet mixers. Specifically, a full factorial design-of-experiments (DOE) study was executed for each mixer with 3 factors and 3 levels (Table 1). The 3 factors investigated cover a process, a formulation, and an excipient parameter, and the study is designed to identify potential interdependent relationships between factors. Experiments were conducted with a single formulation (i.e., the commercial lipid formulation used in Onpattro),[34] with an antisense oligonucleotide (ASO). The measured quality attribute responses included particle size and size distribution measured by dynamic light scattering (DLS), the percentage of ASO encapsulated in the LNP, the extent of order in the LNP core as measured by small-angle X-ray scattering (SAXS) peak positions, and cryogenic electron microscopy (CryoEM). We further evaluated a subset of the DOE with the same formulation, but an mRNA (mRNA) payload. The results from these experiments were statistically and qualitatively compared for each mixer and for each payload to identify trends and understand the translatability of the results across different mixer technologies.

2. EXPERIMENTAL SECTION

2.1. Materials.

DLin-MC3-DMA (MC3, >98%) was obtained from MedChemExpress (Monmouth Junction, NJ). 1,2-Distearoyl-*sn*-glycero-3-phosphatidylcholine (DSPC, >99%), cholesterol (>99%), and 1,2-dimyristoyl-*rac*-glycero-3-methoxypolyethylene glycol-2000 (DMG-PEG2000, >99%) were obtained from Avanti (Alabaster, AL). All lipids were dissolved in ethanol (USP-grade) obtained from Sigma-Aldrich (St. Louis, MO). Sodium chloride, disodium phosphate, monosodium phosphate, and potassium chloride were obtained as USP-grade reagents from Sigma-Aldrich (St. Louis, MO). A 17-mer ASO (M.W. 5635 g/mol, Na-salt form) with a phosphorothioate backbone was custom synthesized by BioSpring GmbH (Frankfurt, Germany) using solid-phase synthesis. A 5-moU modified enhanced green fluorescent protein mRNA (eGFP mRNA, 980 nucleotides) was obtained from GenScript (Piscataway, NJ).

2.2. LNP Formation by Microfluidic Mixing.

Lipids were mixed in ethanol at a fixed total lipid concentration of 10 mM for the ASO-LNP DOE and 2 mM for the mRNA-LNP experiments. A base lipid composition with molar ratios of 50.0:10.0:38.5:1.5 (MC3/DSPC/Cholesterol/DMG-PEG2000) was used, consistent

with the commercial Onpattro formulation. Lipid compositions were varied such that the MC3 content was 50%, 100%, or 150% on a molar basis relative to this base formulation to simulate the incorrect addition of this single component. All other lipids were kept at constant relative ratios. These compositions reflect what would happen if the formulation was prepared correctly except for the ionizable lipid. The molar ratios of lipids in these three compositions correspond to 32.7:13.5:51.8:2.1 (50%), 50.0:10.0:38.5:1.5 (100%), and 59.3:8.2:31.3:1.2 (150%) on a MC3/DSPC/Cholesterol/DMG-PEG2000 basis.

ASO or mRNA was dissolved in an aqueous 10 mM sodium citrate buffer at pH 4.0. The amount of ASO was varied to enable N/P ratios (i.e., the ratio of ionizable amines to phosphates in the backbone of the nucleic acid) of 1, 2, or 6 in the final LNP. These LNP values were based on literature data, where an N/P ratio of 2 was used for ASOs[35] and an N/P ratio of 6 was used for mRNAs.[36] The temperatures of the solutions were not controlled.

LNPs were formed with the ethanol and aqueous phases on a Nanoassemblr Ignite from Precision Nanosystems, Inc. (Vancouver, BC, Canada) with the "Classic" SHM cartridges. Cartridges were used one time and discarded. The ethanol flow rate was fixed at 3 mL/min for all experiments, and the aqueous flow rate was varied to 9, 13.5, or 18 mL/min to enable FRRs of 3:1, 4.5:1, or 6:1, respectively. This resulted in total flow rates of 12, 16.5, or 21 mL/min. A collection volume of 1.4 mL was used, with discard volumes of 0.1 mL (initial) and 0.05 mL (final). Experiments for a subset of the DOE with a greater initial discard volume (0.15 mL) showed no significant difference in the particle size or size distribution. After formation, the LNPs were diluted to approximately 5% (v/v) ethanol with a pH-adjusted 1× phosphate-buffered saline (PBS) solution. Diluted solutions were loaded into centrifugal filtration units from Merck KGaA (Darmstadt, Germany) and centrifuged twice to wash and concentrate the sample. Washing and storage were performed with a 1× PBS solution for ASO-LNPs and with a PBS solution with cryoprotectant for mRNA-LNPs.

2.3. LNP Formation by Coaxial Turbulent Jet Mixing.

Ethanol and aqueous phases were prepared, consistent with section 2.2. LNPs were formed on a LARU unit from DIANT Pharma, Inc. (Manchester, CT), as previously reported.[29] Briefly, an inner tube containing the ethanol phase is positioned concentrically within an outer tube containing the aqueous phase. The two fluids flow in the same direction and mix to form a jet and spontaneously form LNPs downstream in a turbulent mixing region. Unless otherwise noted, the solution temperature was not controlled. The ethanol flow rate was fixed at 20 mL/min for all experiments. The aqueous flow rate was varied as 60, 90, or 120 mL/min to enable FRRs of 3:1, 4.5:1, or 6:1. This resulted in total flow rates of 80, 110, and 140 mL/min. After flow was initiated, flow rates were allowed to equilibrate for approximately 10 s with the solution sent to discard, followed by sample collection for approximately 6 s. This resulted in a collection volume of approximately 8–14 mL and a discard volume of approximately 13–23 mL per run, depending on the total flow rate. The sample collection time can be adjusted from as low as 2 seconds to hours, depending on the desired sample volume. Immediately after formation, the LNPs were diluted in-line to

approximately 5% v/v ethanol with a pH-adjusted PBS solution, and subsequently processed similar to section 2.2 for both the ASO and mRNA LNPs.

2.4. Particle Size and Size Distribution.

The particle size and size distribution were measured as the hydrodynamic diameter (intensity-averaged particle size, *Z*-average, *D*) and polydispersity index (PDI), respectively, on a ZetaSizer Ultra dynamic light scattering (DLS) instrument from Malvern Panalytical (Malvern, UK). Samples were diluted 10× in PBS prior to analysis. Samples produced by the coaxial turbulent jet mixer were analyzed in triplicate. All other samples were measured once. ASO-LNP and mRNA-LNP samples were measured immediately after formation and dilution and again immediately after concentration and solution exchange. Minimal changes in particle size or PDI were observed for ASO-LNPs between these steps, and thus, DLS data were only reported after formation and dilution for these samples. Significant changes in particle size or PDI were observed for mRNA-LNPs after concentration and solution exchange, and thus, DLS data for both measurements were reported.

2.5. Nucleic Acid Concentration.

Free ASO (i.e., unencapsulated) concentrations in each formulation were quantified using the Quant-iT Oligreen ssDNA assay from Thermo Fisher Scientific (Waltham, MA). Total ASO concentrations were quantified with the same assay after LNP disruption at 37 °C using 0.2% RNase-free Triton X-100 from Millipore Sigma (St. Louis, MO). The determined free and total ASO concentrations were used to calculate the percentage of encapsulated (%E) ASO for samples after dilution. The %E mRNA and mRNA concentrations were similarly determined using the Quant-iT RiboGreen RNA assay from Thermo Fisher Scientific (Waltham, MA). ASO-LNP and mRNA-LNP samples were measured immediately after formation and dilution to measure the encapsulation efficiency from the mixing process.

2.6. Small-Angle X-ray Scattering (SAXS) Measurement.

SAXS data were collected in the high throughput mode (HT-SAXS) using the Advanced Light Source SIBYLS beamline 12.3.1 at the Lawrence Berkeley National Laboratory (Berkley, CA), as reported previously.[35,37,38] The X-ray wavelength was set at λ = 1.216 Å, and the sample-to-detector distance was 2070 mm, resulting in a scattering vector, q, ranging from 0.01 $Å^{-1}$ to 0.45 $Å^{-1}$. The scattering vector is defined as $q = 4\pi \sin \theta/\lambda$, where 2θ is the scattering angle. Experiments were performed at 20 °C as described elsewhere. Briefly, the sample was exposed for 10 s with the detector framing at 0.3 s to maximize the signal while merging the SAXS signal using the SAXS FrameSlice application (https://bl1231.als.lbl.gov/ran). No radiation damage was observed during the 10 s exposure, and all of the collected frames were merged. The merged SAXS profile was further processed using BioXTAS RAW (https://bioxtas-raw.readthedocs.io/en/latest/index.html) and OriginPro 2022b from OriginLab Corporation (Northampton, MA). All SAXS curves are available at simplescattering.com under entry XS0ZP76H.

The SAXS scattering profiles were set to a consistent baseline to account for scattering profiles with intensities that decreased dramatically at high *q*. The profiles were then

processed using Batch Peak Analysis on OriginPro to identify the position of the first observable peak. The baseline for the peak search was determined by a straight line that connects the data at $q = 0.05$ and 0.3. Subsequently, the baseline was subtracted, the data was rescaled and smoothed using the Savitzky–Golay method with a polynomial order of 2 and points of window of 20, and a peak search algorithm was applied to identify the q position of the q_0 peak via the first derivative of the data and height threshold of 60%. Our study restricted analysis of the SAXS data to quantification of a single peak position. Literature reports show that multiple types of order may be present in samples, which can lead to broad or asymmetric peaks that may not be fully described by a single peak position.[38] Deeper analysis may provide additional insight.

Twenty-seven SAXS measurements were made for each mixer, one for each combination of FRR, N/P ratio, and MC3 content, for a total of 54 measurements. All SAXS measurements were performed on samples after dilution, concentration, and solution exchange. Samples were analyzed after storage at 2–8 °C for up to 1 week but most commonly within 2 days. Samples were loaded into a 96-well plate without further manipulation for measurement.

2.7. Cryo Electron Microscopy (CryoEM) Imaging.

Quantifoil-Cu300 R1.2/1.3 + 2 nm carbon grids were discharged for 9 s on a CEMRC GloQube at 20 mA and prepared on the CEMRC Vitrobot Mark IV set to 4 °C/95% humidity. Excess liquid was blotted using a blot force of −11, a wait time of 45 s, and a drain time of 0.5 s for all grids. All images were collected on a Talos Arctica 200 keV TEM equipped with a Falcon III camera. Images were collected from holes distributed across the overview maps. Select holes were imaged at lower magnification with 3.39 Å/pixel and a defocus range −4.0 to −2.0 μm with a total 15 $e^{-}/Å^2$ electron dose. Images were collected at higher magnification with a 0.96 Å/pixel and a defocus range of −2.0 to −3.0 μm, or a 0.78 Å/pixel and a defocus of −1.5 μm with a total 57 $e^{-}/Å^2$ electron dose.

All CryoEM measurements were performed on samples after dilution, concentration, and solution exchange. Samples were frozen after storage at 2–8 °C for up to 1 week but most commonly within 2 days.

CryoEM images were manually counted for the frequency of the bleb features in each sample. At least 300 images were counted per sample across multiple regions of the grid. While the data may not quantitatively correlate to bulk measurements, the results can be used directionally to inform the relative amounts of each sample.

2.8. Lipid Measurement.

Briefly, the LNP samples were diluted 20× (v/v) with ethanol and then vigorously vortexed and analyzed by liquid chromatography–mass spectrometry (LC-MS). The lipids were quantified by using an external calibration standard.

A Thermo Fisher Scientific (Sunnyvale, CA) LC-MS system was composed of an UltiMate 3000 Rapid Separation (RS) dual-pump module containing two ternary pumps, an RS autosampler, a thermostatic RS column compartment, and an ISQ EC single-quadrupole mass spectrometer equipped with a heated electrospray ionization (HESI) ion source. A

BioResolve RP mAb Polyphenyl column (2.7 μm, 100 × 2.1 mm, 450 Å) was purchased from Waters Corporation (Milford, MA).

The mobile phases contained 10 mM ammonium acetate in water (mobile phase A) or 1:1 methanol/2-propanol by volume (mobile phase B). The lipids were eluted by increasing the mobile phase B composition from 25% to 100% in 3.5 min. The column temperature was set to 40 °C, and the flow rate was set to 0.6 mL/min. The HESI parameters were as follows: spray voltage, +3.0 kV; vaporizer temperature, 282 °C; ion transfer tube temperature, 300 °C; sheath gas, auxiliary gas, and sweep gas flow rates, 49.9, 5.7, and 0.5 psig, respectively. The ISQ EC mass spectrometer was operated in selective ion monitoring (SIM) mode.

2.9. Design of Experiments (DOE) Analysis.

The JMP software (V16.1.0) from SAS was used to develop statistical models for experimental design and the investigated factors. Interaction terms were analyzed for statistical significance ($p < 0.05$). The results from the experiments were analyzed using standard least-squares analysis with emphasis set as effect screening, fitting one response at a time to determine the significance of the model effects. A quadratic response surface model was preformed to help minimize the sum of squares of the residuals. Partial least-squares regression analysis was used to attain minimal variation for the coefficients and reduce the prediction errors of the model. The analysis of variance (ANOVA) was conducted to determine the effectiveness of the model based on R^2 and Q^2 as the goodness of fit and prediction, respectively. The R^2 values are referenced throughout the text as a measure of how well the responses in each data set correlate with the investigated factors, where R^2 values approaching 1 indicate a better fit. Response contour plots (2D) were used for model analysis and the identification of optimal operating regions in the predictive model.

3. RESULTS

3.1. ASO-LNP DOE.

3.1.1. DOE with Coaxial Turbulent Jet Mixer.—

LNP preparation with the coaxial turbulent jet mixer yielded LNPs with a narrow size distribution that encapsulate ASO with high efficiency over a broad design space (Figure 1; Table S1). Select samples from disparate regions of the DOE design space were analyzed for lipid content by HPLC-MS (Table S2). All analyzed lipid compositions were consistent with the target composition. Analysis of lipid content before and after downstream processing showed that the composition was maintained and that lipids were recovered in high yield (>85%) relative to expected values. These data indicate that the investigated compositions carry forward from the lipid stocks to the finished product.

Analysis of ASO encapsulation data, as measured by the Quant-iT Oligreen assay, showed that over 70% of samples had %E greater than or equal to 85%, with less than 10% of samples below 70%. The predicted model for %E showed an R^2 correlation of 0.49, with N/P as the only significant factor (Figure S1a). Specifically, an increase in %E was observed with an increased N/P ratio (Figure 1c). We hypothesize that increased ionizable lipid

content increases ASO-ionizable lipid interactions upon mixing, which leads to greater ASO encapsulation during LNP formation.

Particle size, as measured by DLS, varied between 50 and 80 nm (with one exception), with a median of approximately 65 nm. The predicted model for particle size showed an R^2 correlation of 0.78, with MC3, FRR*MC3, and MC3*MC3 as significant factors (Figure S2a). Specifically, particle size increased with MC3 content, but was relatively insensitive to FRR and N/P (Figure 1a). All samples had PDI values less than or equal to 0.22, and 70% of the samples had PDI values less than or equal to 0.1. The predicted model for PDI was relatively insensitive to the investigated factors, with an R^2 correlation of 0.46 (Figures 1b and S3a).

To further understand changes in the internal LNP structure that may not be captured by DLS, we additionally measured samples by SAXS (Figure 1d). Specifically, the center point of the first peak observed (i.e., q_0) was measured and used to inform relative differences in structure. A broad q_0 peak centered at 0.090–0.100 $Å^{-1}$ was tentatively assigned to represent a disordered core structure. As the extent of order within the core increases, the q_0 peak shifts to 0.115–0.130 $Å^{-1}$. The assignment of these peaks and observed q_0 values are consistent with previous literature examples of ASO-LNPs analyzed with SAXS.[35,38] The predicted model for q_0 showed an R^2 correlation of 0.89, with N/P identified as a significant factor (Figure S4a). Specifically, as N/P was increased, a q_0 peak shift to lower q was observed, which suggests a loss of internal order (Figures 1d and S5).

To better understand the structural changes observed by SAXS, CryoEM analysis was performed on select samples (Figures 1e and S6; Table S3). CryoEM analysis showed a transition from dense ordered cores with a moderate frequency of large aqueous blebs (~25%) at the low corner of the design space (−1, −1, −1; or low FRR, low N/P, low MC3 content), to similar cores with a lower frequency (~15%) of smaller aqueous blebs at the center point (0, 0, 0), to disordered cores with a high frequency of aqueous blebs (~65%) at the high corner (1, 1, 1). These trends of decreased order with increased N/P and MC3 content are consistent with SAXS observations and support our assignment of a broad q_0 peak to a disordered core structure. A similar trend from ordered to disordered cores was observed with increased N/P ratio for siRNA-LNP formulations prepared with a T-junction mixer, albeit without the bleb features.[14,15] We hypothesize that as N/P (and MC3 content) increases, the excess ionizable lipid engages in lipid–lipid interactions, rather than ASO–lipid interactions, which results in a disordered phase in the LNP core.

3.1.2. Investigation of Temperature Control with Coaxial Turbulent Jet.—

The temperature of the feed and outlet streams can also be controlled and directly measured in the flow for the investigated coaxial turbulent jet mixer. For small-scale commercially available microfluidic mixing technologies, such as the Nanoassemblr Ignite used in this article, the feed solutions can be heated, but not cooled, and the solution temperature is not directly measured. For larger scale microfluidic mixing technologies, the temperature may be more readily controlled and monitored.

To investigate whether temperature has an impact on LNP formation, two conditions from the DOE were selected and evaluated at four aqueous feed stream temperatures: 5, 25, 40, and 60 °C (Figure S7). When these data were evaluated, no clear trends in particle size or PDI were observed as a function of temperature. While the data set is small, and the result may not be statistically significant, %E was observed to increase with increased temperature. We hypothesize that mixing is less efficient at lower temperatures and thus may result in decreased levels of ASO encapsulation. For cargos sensitive to temperature-dependent chemical degradation, it may thus be preferable to mix at room temperature, but use refrigerated solutions for subsequent process steps.

3.1.3. ASO-LNP DOE with Microfluidic Mixer.—LNP preparation with the microfluidic mixer yielded comparatively larger LNPs with a broader particle size distribution that encapsulate ASO with lower efficiency (Figure 2; Table S4). Specifically, only 55% of the samples had %E greater than or equal to 85%, and over 20% of samples were below 70% (Figure 2c). The predicted model for %E showed an R^2 of 0.58 with N/P and N/P*N/P as significant factors (Figure S1b). The %E data followed a trend similar to that of the coaxial turbulent jet mixer.

Particle size varied between 60 to 110 nm (with one exception), with a median particle size of 85 nm (Figure 2a). The predicted model for particle size showed an R^2 correlation of 0.57, with N/P*N/P and MC3 content as significant factors (Figure S2b). Specifically, particle size increased with MC3 content, but was relatively insensitive to FRR and N/P, like the coaxial turbulent jet mixer. PDI values spanned up to 0.5, with 20% of samples above 0.3 and 40% of samples less than or equal to 0.1 (Figure 2b). The predicted model for PDI showed an R^2 of 0.67, with N/P and N/P*N/P also as significant factors, like %E (Figure S3b). The limited sensitivity of the measured responses to FRR above 3:1 is consistent with previous reports and is likely due to the minimal differences in diffusion rate on mixing.[19,24,26]

When analyzed by SAXS, the observed trends are similar to those of LNPs prepared with the coaxial turbulent jet (Figures 2d and S5). However, LNPs produced with the microfluidic mixer retain ordered core structures across a wider design space. The predicted model for the q_0 position measured by SAXS showed that N/P*N/P had significance, with an R^2 correlation of 0.69 (Figure S4b). When select samples were examined by CryoEM, the LNP structure appeared very similar to those produced via the coaxial turbulent jet mixer for the low corner (−1, −1, −1) of the design space (Figures 2e and S8; Table S3). However, the structure looks different for the center point (0, 0, 0) and the high corner (1, 1, 1) of the design space. Specifically, at the center point, there is a lower frequency of aqueous bleb features (<10%) and clear multilamellar features at the outer edge of the particles. The more defined lamellar features are likely the primary structural feature observed in the SAXS data.[38] At the high corner, the LNPs prepared with the microfluidic mixer appear to maintain an ordered core, consistent with the SAXS data, but with a significant fraction of nonspherical particle shapes and smaller, less frequent (~25%) bleb features.

3.1.4. ASO-LNP Experiments at Lower Lipid Concentration.—In early stage research, screening large numbers of LNP formulations can consume significant amounts

of material. If materials are costly or limited in quantity, then this can represent a challenge. Consequently, scale-down models that consume less material are critical to investigate. For many mixing technologies, it can be difficult to decrease the total volumes used due to practical limitations or changes in the physics of mixing. An alternative approach to consuming less material for early stage screens is to decrease the reagent concentrations that are used.

To investigate the impact of reagent concentration, the lipid concentrations were decreased from 10 to 2 mM for two different formulations from the center point and high corner of DOE (Table S5). For both mixers and both formulations evaluated, we generally found comparable particle size, particle size distribution, and encapsulation efficiency. This result suggests that the ASO-LNP DOE results collected at 10 mM lipid concentration may extend to a 5 times lower concentration for both mixer technologies; however, additional data may be required to confirm this conclusion. It is also worth noting that materials formulated at lower lipid concentration may require further concentration steps to enable in vitro or in vivo experiments at comparable dose levels.

3.2. mRNA-LNP Formulation.

Three conditions from the ASO-LNP DOE were replicated for mRNA-LNP formulations to see how translatable the trends were from ASO to mRNA cargoes (Figures 3, S9, and S10 and Tables S6 and S7). In these experiments, all formulation and process parameters were kept constant, except the lipid concentration was dropped from 10 mM to 2 mM to conserve mRNA. These three conditions represent the low (−1, −1, −1), center-point (0, 0, 0), and high (1, 1, 1) conditions of the investigated LNP design space.

For the three conditions investigated, particle size and PDI were comparable for LNPs produced by either mixer. The particle size increased, the PDI decreased, and the %E increased for the high condition (1, 1, 1), likely due to the greater extent of encapsulation with higher N/P and MC3 content.

LNPs produced via both mixers showed a trend in particle morphology observed by CryoEM from a dense disordered core at the low condition (−1, −1, −1), to low contrast disordered cores at the center-point (0, 0, 0) and the high condition (1, 1, 1). Interestingly, LNPs produced via the coaxial turbulent jet mixer showed consistently more frequent blebs as compared to the microfluidic mixer, which appeared as dense mRNA-loaded features (Table S7).[39,40]

4. DISCUSSION

4.1. Comparative Evaluation of LNP Mixer Technologies.

As the pharmaceutical industry invests in LNP research and development, new technologies to manufacture LNPs continue to emerge. These new technologies present a dilemma for interested pharmaceutical or biotechnology companies. If interested companies are early in their development, then a comparative evaluation of multiple manufacturing technologies may be worth the investment. In contrast, if companies have invested in infrastructure and resources to support a particular technology, then speculative evaluation may encounter

internal resistance unless there is a gap or deficiency in their current technologies. If comparative evaluation of different manufacturing technologies is considered worthy of investment, then the study design is critical to maximize the amount of actionable data that is generated.

In this comparative evaluation of ASO-LNP formation, we selected a full-factorial DOE design based on three factors. Through this comprehensive approach, we aimed to compare process robustness, or the ability for a given process to tolerate variability in the selected factors, for two mixers of different design. In this way, the study can serve as a first-pass evaluation of whether process understanding built with one mixer technology can be applied to another, or whether unique development work must be undertaken. To the best of our knowledge, this is the first time that such a controlled study has been reported in the literature, and we hope that this serves as a guide for future evaluations. The design of the DOE study also reflects how one might evaluate manufacturing robustness to inform the design of a pharmaceutical control strategy.

While we attempted to control as many variables as possible in this evaluation, the reported results do have a few limitations, which may limit the generality of the findings. First, a single formulation was tested with a single ASO and a single mRNA. Consequently, the observed trends and optimal conditions may be specific to the investigated conditions (e.g., the lipid composition or cargo that was used). Second, experimental conditions were matched as closely as possible between studies, but in certain cases, this was not possible. For example, the TFRs, sample volumes, and discard volumes were different for each mixer but were selected within the ideal operating windows for each mixer (see sections 2.2 and 2.3). Third, a single mixer geometry was evaluated for each technology, based on commercial availability. Results may not be generally translatable to other mixer geometries (e.g., toroidal microfluidic mixers). Fourth, three parameters associated with mixing were investigated in this study. Additional parameters such as the buffer composition, total flow rate, lipid concentration, or lipid composition may also be critical to LNP formation and may need to be investigated during formulation and process optimization. Last, conclusions are drawn from an analytical comparison of physicochemical and structural properties. However, this manufacturing-focused approach may not correlate with in vitro and in vivo performance.

4.2. Comparison of Coaxial Turbulent Jet and Microfluidic Mixers.

To compare the results produced via the two different mixing technologies, ASO-LNP data for matched preparation conditions were plotted for each quality attribute analyzed in the DOE (Figure 4). If direct correlation between mixers was observed for a given set of formulation and process conditions, then we would expect the data to fall along the dashed line in each graph. If the data deviate from this dashed line, then the direction and magnitude of the deviations inform relative differences between mixing technologies. From this evaluation, particle size is consistently smaller, and the particle size distribution is consistently narrower for samples produced via the coaxial turbulent jet mixer (Figure 4a,b). ASO encapsulation is also consistently higher for samples produced via the coaxial turbulent jet mixer (Figure 4c). The q_0 position is consistently shifted to higher values for

the microfluidic samples, reflective of core structures with greater internal order (Figure 4d). When the data are segmented and analyzed by each factor, N/P has a significant effect on the measured physicochemical properties, with the greatest discrepancies between mixers at N/P = 1 (Figure S11).

Cullis and co-workers hypothesized that on mixing, LNP formation is initiated through electrostatic interactions between positively charged ionizable lipids and negatively charged nucleic acids.[1,20] This interaction drives the formation of an inverted micelle containing nucleic acid, surrounded predominantly by an ionizable lipid. As the solvent polarity increases with further mixing of the aqueous and organic solutions, inverted micelles may precipitate out of solution. If mixing occurs faster than inverted micelle aggregation, then the lipopolymer will precipitate at higher solvent polarity and coat the inverted micelles. If mixing occurs relatively slowly, then inverted micelles may aggregate before the lipopolymer can precipitate out. In this slower mixing scenario, LNP formation may occur around inverted micelles in various states of aggregation, which could lead to larger particle sizes and a broader size distribution. At low N/P values, the risk of aggregation is likely exacerbated, as there are fewer ionizable lipids per ASO, and thus the driving force for ASO-ionizable lipid interactions may be reduced. We hypothesize that the higher TFR and turbulent mixing produced by the coaxial turbulent jet mixer enable faster mixing compared to the microfluidic mixer and that this faster mixing yields smaller LNPs with a narrower particle size distribution. This hypothesis is supported by literature, where decreases in particle size and particle size distribution have been seen for liposomes, polymeric nanoparticles, and inorganic nanoparticles produced via coaxial turbulent jet mixing compared to other mixers.[28,29] Particle size has been previously shown to have a significant impact on biodistribution, immunogenicity, and activity, and thus these differences could have a significant impact on in vivo performance.[8,11]

Beyond statistical comparisons of matched conditions, there are distinct trends in the internal structure of LNPs prepared with each mixer technology that merit further discussion. Specifically, ASO-LNPs produced with the coaxial turbulent jet mixer possess less ordered cores on average as measured by SAXS and CryoEM, and most matched ASO-LNPs and mRNA-LNPs produced by the coaxial turbulent jet mixer possess more aqueous blebs as visualized by CryoEM (Figures 4d, S5, S6, S8, and S12). We hypothesize that the inertial forces generated in the turbulent mixing conditions may disrupt LNP formation, and cause more frequent bleb formation as compared to the laminar flow conditions of the microfluidic mixers. We further hypothesize that the more ordered cores observed in LNPs prepared with the microfluidic mixer may originate from the larger particle size, which imposes less steric hindrance and curvature that could limit ordered phase formation. Alternatively, less ordered cores could indicate a greater fraction of "empty" LNPs that do not contain nucleic acid.[41] Our understanding of the relationship between internal structure and performance is still growing, but one could imagine that internal structure could represent a critical quality attribute that impacts endosomal escape and target knockdown or expression. For example, in a recent publication, the formation of ordered phases in ASO-LNPs with different formulations was found to correlate with in vitro gene silencing efficacy.[38]

These data have several critical implications for the design and manufacture of ASO-LNPs, albeit with the caveats listed at the start of the discussion section. First, over the investigated design space, there is less variation in particle size, particle size distribution, and encapsulation for the coaxial turbulent jet mixer compared to the microfluidic mixer. This might suggest that the control strategy for LNP manufacturing with a coaxial turbulent jet mixer may accommodate wider operating ranges for the investigated formulation and process parameters. Second, LNPs produced via the coaxial turbulent jet mixer are smaller and more uniform. Such differences could have potential benefits to downstream unit operations, such as sterile filtration, and result in more consistent in vivo behavior, as particle size has been shown to impact in vivo performance.[8,11] Third, the higher encapsulation efficiency and lower ionizable lipid requirements (i.e., ability to form similar structures at lower N/P) for the coaxial turbulent jet mixer could lead to potential cost savings, especially for mRNA payloads. When improvements in product quality are combined with the reduced cost of consumables and the integration into a continuous process train with in-process analytics, the coaxial turbulent jet mixer technology may be positioned well for process scale-up and manufacture to support clinical and commercial development.

Despite the benefits listed above, it is worth noting that the minimum volumes used are over an order of magnitude greater for the coaxial turbulent jet mixer compared to other LNP mixer technologies. For research applications, where material is limited or where a larger design space is investigated, the greater volumes associated with the coaxial turbulent jet mixer may be prohibitive. Innovations in the mixer design and a decrease in lipid concentrations (as was used for the mRNA experiments) may reduce volume requirements and support investigations at smaller scales in the future. At present, researchers may prefer to initiate research with an alternative mixer (e.g., high-throughput mixer,[42,43] microfluidic mixer, or impinging jet mixer) and transfer their formulation and process over to the coaxial turbulent jet mixer when larger scale production is required.

If a process is transferred between mixer technologies, then comparability assessments will be required to determine whether LNPs are of similar quality and functionality. To evaluate whether matched formulation and process conditions can produce LNPs with comparable physicochemical properties, we developed statistical models for each measured quality attribute based on ASO-LNP data sets from each mixer individually and in combination (Figures S1c and S4c; Table S8). The most significant statistical model observed from the combined data set was for the q_0 position as measured by SAXS, where an R^2 of 0.67 was predicted, with N/P identified as a significant factor. The R^2 values for models built from the combined data set for encapsulation, particle size, and particle size distribution were lower than for models built from the individual mixer data sets (0.42, 0.33, and 0.31, respectively; Table S8). A weak statistical correlation for the other models built with the combined data set does not necessarily mean that LNPs with comparable physicochemical properties cannot be prepared from each mixer. Instead, this result indicates that formulation and process variables likely need to be modified for each mixer to achieve comparable physicochemical properties. Functional assessments of biological activity may be required to understand the criticality of each physicochemical property and how much difference in the property can be tolerated.

4.3. Comparison of ASO and mRNA LNPs.

LNP structure is impacted by the encapsulated cargo, formulation, and process parameters.[25,36,39,40] However, there are few studies that directly compare LNP formation under identical formulation and process conditions with ASO and mRNA cargoes. Consequently, it can be difficult to infer how much the structures differ due to differences in the study design or the cargo itself. In this case, the Onpattro formulation was optimized for a siRNA and may not necessarily be optimal for ASOs or mRNAs. It is also worth noting that the size of the mRNA-LNP data set is much smaller than that of the ASO-LNPs, so comparisons are less quantitative.

We observed that the particle size is significantly smaller for an ASO-LNP as compared to an mRNA-LNP for matched conditions. For both cargos, we observed that LNP structures trended from dense, ordered cores at the low condition (−1, −1, −1) to more disordered cores at the high condition (1, 1, 1). However, we found that the transition points between these extreme structures were different. ASO-LNPs remained as ordered cores at a higher N/P and MC3 content. We hypothesize that the observed differences are due to the size of the cargo. Specifically, the smaller ASO appears to be more readily accommodated in the core of the LNP without a significant expansion in particle size, which may arise due to disruption of the internal order or bleb formation. By contrast, we hypothesize that small increases in N/P and MC3 content can increase the mRNA loading per particle and cause significant disruptions in structure.

When CryoEM images of ASO- and mRNA-LNP samples under matched conditions are compared, we see a significant difference in the visible appearance of the blebs. Specifically, the blebs observed in ASO-LNPs are lower contrast than those in mRNA-LNPs. In the literature, this visual difference in bleb appearance has been attributed to nucleic acid loaded into blebs, where the terms "aqueous" and "nucleic-acid loaded" blebs refer to low- and high-contrast blebs in CryoEM images, respectively.[39,40] Further investigation is required to confirm whether the "aqueous" blebs observed in ASO-LNPs indeed lack nucleic acid. The presence of blebs, regardless of the type, have historically been hypothesized to arise from the presence of larger mRNAs that cannot be as easily accommodated into ordered lipid cores.[25,36,39,40] Here, we observe that the mixer technology impacts the frequency of blebs observed by CryoEM, while the cargo impacts whether the bleb appears loaded with nucleic acid. This finding suggests that blebs may originate in part from mixing conditions in conjunction with formulation and cargo, but further studies are required to confirm this result. Further investigation is also required to understand the impact of these features on the in vitro and in vivo activities of the LNPs.

5. CONCLUSION

In this paper, we showed that the mixer technology used to manufacture LNPs can have a significant impact on LNP physicochemical and structural properties. We found that each mixer technology could produce LNPs with high nucleic acid encapsulation, but the particle size, particle size distribution, and internal core structure of these LNPs differed significantly. ASO-LNPs produced via the coaxial turbulent jet mixer were smaller and had a narrower particle size distribution, less ordered cores, and a greater frequency of bleb

features compared to ASO-LNPs produced via a SHM microfluidic mixer. Furthermore, we found that for both mixers, N/P had a significantly greater impact on the physicochemical and structural properties of ASO-LNPs, compared to the ionizable lipid content or FRR, over the investigated ranges. We encourage researchers to investigate how translatable these findings are to other LNP compositions and to expand beyond the investigated design space to inform process optimization.

The study design provides a roadmap for how researchers may collect comparative data for different mixing technologies, and the data collected highlight the importance of assessments beyond particle size and encapsulation. If researchers intend to transfer a formulation and process between mixer technologies, then such studies can inform whether LNPs with comparable physicochemical attributes can be formed and, if so, how much formulation and process modification is required. Based on the size and systematic nature of the data sets collected, we were also able to demonstrate that the mixer technology can impact process robustness to intentional variations in formulation and process parameters. As researchers progress LNP programs into clinical and commercial development, process robustness can impact multiple elements of manufacturing control strategies, such as the identification of critical parameters and the determination of specifications.

Ultimately, this CMC-focused evaluation must be paired with appropriate in vitro and in vivo assessments to understand whether differences in physicochemical and structural properties impact biological activity. With those inputs, a suitable control strategy can be designed accordingly. The selection of an optimal mixer technology may ultimately depend on unique in vivo considerations for a given target and indication. We encourage formulation scientists and process engineers to perform comparable systematic assessments with their intended formulation and process to develop process understanding, identify critical parameters, and design appropriate control strategies for LNP manufacture.

Supplementary Material

Refer to Web version on PubMed Central for supplementary material.

ACKNOWLEDGMENTS

The authors thank Karthik Nagapudi for support of this research and valuable feedback on the manuscript. CryoEM imaging was performed in the CryoEM Research Center (CEMRC) in the Department of Biochemistry at the University of Wisconsin-Madison. All SAXS data was collected at the SIBYLS Advanced Light Source beamline which operates through support from the following sources: National Institute of Health grant ALS-ENABLE (P30 GM124169), National Cancer Institute grant SBDR (CA92584), Department of Energy through Basic Energy Science grant DE-AC02-05CH11231 and Biological and Environmental Research grant IDAT.

ABBREVIATIONS

ASO	antisense oligonucleotide
CryoEM	cryogenic electron microscopy
DLS	dynamic light scattering
DOE	design of experiments

FRR	flow rate ratio
LNP	lipid nanoparticle
mRNA	messenger ribonucleic acid
PDI	polydispersity index
SAXS	small-angle X-ray scattering
SHM	staggered herringbone micromixer
TFR	total flow rate

REFERENCES

(1). Cullis PR; Hope MJ Lipid Nanoparticle Systems for Enabling Gene Therapies. Mol. Ther 2017, 25, 1467–1475. [PubMed: 28412170]

(2). Adams D; Gonzalez-Duarte A; O'Riordan WD; et al. Patisiran, an RNAi Therapeutic, for Hereditary Transthyretin Amyloidosis. New England Journal of Medicine 2018, 379, 11–21. [PubMed: 29972753]

(3). Baden LR; El Sahly HM; Essink B; et al. Efficacy and Safety of the mRNA-1273 SARS-CoV-2 Vaccine. New England Journal of Medicine 2021, 384, 403–416. [PubMed: 33378609]

(4). Polack FP; Thomas SJ; Kitchin N; et al. Safety and Efficacy of the BNT162b2 mRNA Covid-19 Vaccine. New England Journal of Medicine 2020, 383, 2603–2615. [PubMed: 33301246]

(5). Thomas SJ; Moreira ED; Kitchin N; et al. Safety and Efficacy of the BNT162b2 mRNA Covid-19 Vaccine through 6 Months. New England Journal of Medicine 2021, 385, 1761–1773. [PubMed: 34525277]

(6). Hou X; Zaks T; Langer R; et al. Lipid nanoparticles for mRNA delivery. Nat. Rev. Mater 2021, 6, 1078–1094. [PubMed: 34394960]

(7). Kauffman KJ; Dorkin JR; Yang JH; et al. Optimization of Lipid Nanoparticle Formulations for mRNA Delivery in Vivo with Fractional Factorial and Definitive Screening Designs. Nano Lett 2015, 15, 7300–7306. [PubMed: 26469188]

(8). Chen S; Tam YYC; Lin PJC; et al. Influence of particle size on the in vivo potency of lipid nanoparticle formulations of siRNA. J. Controlled Release 2016, 235, 236–244.

(9). Hassett KJ; Benenato KE; Jacquinet E; et al. Optimization of Lipid Nanoparticles for Intramuscular Administration of mRNA Vaccines. Mol. Ther. Nucleic 2019, 15, 1–11.

(10). Cheng Q; Wei T; Farbiak L; Johnson LT; Dilliard SA; Siegwart DJ Selective organ targeting (SORT) nanoparticles for tissue-specific mRNA delivery and CRISPR–Cas gene editing. Nat. Nanotechnol 2020, 15, 313–320. [PubMed: 32251383]

(11). Hassett KJ; Higgins J; Woods A; et al. Impact of lipid nanoparticle size on mRNA vaccine immunogenicity. J. Controlled Release 2021, 335, 237–246.

(12). Tahtinen S; Tong A-J; Himmels P; et al. IL-1 and IL-1ra are key regulators of the inflammatory response to RNA vaccines. Nat. Immunol 2022, 23, 532–542. [PubMed: 35332327]

(13). Zhang Y; Sun C; Wang C; et al. Lipids and Lipid Derivatives for RNA Delivery. Chem. Rev 2021, 121, 12181–12277. [PubMed: 34279087]

(14). Kulkarni JA; Darjuan MM; Mercer JE; et al. On the Formation and Morphology of Lipid Nanoparticles Containing Ionizable Cationic Lipids and siRNA. ACS Nano 2018, 12, 4787–4795. [PubMed: 29614232]

(15). Kulkarni JA; Witzigmann D; Leung J; et al. On the role of helper lipids in lipid nanoparticle formulations of siRNA. Nanoscale 2019, 11, 21733–21739. [PubMed: 31713568]

(16). Semple SC; Akinc A; Chen J; et al. Rational design of cationic lipids for siRNA delivery. Nat. Biotechnol 2010, 28, 172–176. [PubMed: 20081866]

(17). Jayaraman M; Ansell SM; Mui BL; et al. Maximizing the Potency of siRNA Lipid Nanoparticles for Hepatic Gene Silencing In Vivo**. Angew. Chem., Int. Ed 2012, 51, 8529–8533.

(18). Ferhan AR; Park S; Park H; et al. Lipid Nanoparticle Technologies for Nucleic Acid Delivery: A Nanoarchitectonics Perspective. Adv. Funct. Mater 2022, 32, 2203669.

(19). Ripoll M; Martin E; Enot M; Robbe O; Rapisarda C; Nicolai M-C; Deliot A; Tabeling P; Authelin J-R; Nakach M; Wils P Optimal self-assembly of lipid nanoparticles (LNP) in a ring micromixer. Sci. Rep 2022, 12, 9483. [PubMed: 35676394]

(20). Belliveau NM; Huft J; Lin PJC; et al. Microfluidic Synthesis of Highly Potent Limit-size Lipid Nanoparticles for In Vivo Delivery of siRNA. Mol. Ther. Nucleic 2012, 1, e37.

(21). Evers MJW; Kulkarni JA; van der Meel R; et al. State-of-the-Art Design and Rapid-Mixing Production Techniques of Lipid Nanoparticles for Nucleic Acid Delivery. Small Methods 2018, 2, 1700375.

(22). Maeki M; Uno S; Niwa A; et al. Microfluidic technologies and devices for lipid nanoparticle-based RNA delivery. J. Controlled Release 2022, 344, 80–96.

(23). Capretto L; Cheng W; Hill M; Zhang X Micromixing Within Microfluidic Devices. Top. Curr. Chem 2011, 304, 27–68. [PubMed: 21526435]

(24). Terada T; Kulkarni JA; Huynh A; et al. Characterization of Lipid Nanoparticles Containing Ionizable Cationic Lipids Using Design-of-Experiments Approach. Langmuir 2021, 37, 1120–1128. [PubMed: 33439022]

(25). Leung AKK; Tam YYC; Chen S; et al. Microfluidic Mixing: A General Method for Encapsulating Macromolecules in Lipid Nanoparticle Systems. J. Phys. Chem. B 2015, 119, 8698–8706. [PubMed: 26087393]

(26). Roces CB; Lou G; Jain N; et al. Manufacturing Considerations for the Development of Lipid Nanoparticles Using Microfluidics. Pharmaceutics 2020, 12, 1095. [PubMed: 33203082]

(27). Shepherd SJ; Warzecha CC; Yadavali S; et al. Scalable mRNA and siRNA Lipid Nanoparticle Production Using a Parallelized Microfluidic Device. Nano Lett 2021, 21, 5671–5680. [PubMed: 34189917]

(28). Lim J-M; Swami A; Gilson LM; et al. Ultra-High Throughput Synthesis of Nanoparticles with Homogeneous Size Distribution Using a Coaxial Turbulent Jet Mixer. ACS Nano 2014, 8, 6056–6065. [PubMed: 24824296]

(29). Costa AP; Xu X; Khan MA; et al. Liposome Formation Using a Coaxial Turbulent Jet in Co-Flow. Pharm. Res 2016, 33, 404–416. [PubMed: 26428671]

(30). Gupta A; Costa AP; Xu X; et al. Formulation and characterization of curcumin loaded polymeric micelles produced via continuous processing. Int. J. Pharm 2020, 583, 119340. [PubMed: 32305363]

(31). Gupta A; Costa AP; Xu X; et al. Continuous processing of paclitaxel polymeric micelles. Int. J. Pharm 2021, 607, 120946. [PubMed: 34333023]

(32). Yenduri G; Costa AP; Xu X; et al. Impact of critical process parameters and critical material attributes on the critical quality attributes of liposomal formulations prepared using continuous processing. Int. J. Pharm 2022, 619, 121700. [PubMed: 35358645]

(33). Troiano G; Nolan J; Parsons D; et al. A Quality by Design Approach to Developing and Manufacturing Polymeric Nanoparticle Drug Products. AAPS Journal 2016, 18, 1354–1365. [PubMed: 27631558]

(34). Akinc A; Maier MA; Manoharan M; Fitzgerald K; Jayaraman M; Barros S; Ansell S; Du X; Hope MJ; Madden TD; et al. The Onpattro story and the clinical translation of nanomedicines containing nucleic acid-based drugs. Nat. Nanotechnol 2019, 14, 1084–1087. [PubMed: 31802031]

(35). Sarode A; Fan Y; Byrnes AE; et al. Predictive high-throughput screening of PEGylated lipids in oligonucleotide-loaded lipid nanoparticles for neuronal gene silencing. Nanoscale Adv 2022, 4, 2107–2123. [PubMed: 36133441]

(36). Schoenmaker L; Witzigmann D; Kulkarni JA; et al. mRNA-lipid nanoparticle COVID-19 vaccines: Structure and stability. Int. J. Pharm 2021, 601, 120586. [PubMed: 33839230]

(37). Dyer KN; Hammel M; Rambo RP; et al. High-throughput SAXS for the characterization of biomolecules in solution: a practical approach. Methods Mol. Biol 2014, 1091, 245–258. [PubMed: 24203338]

(38). Hammel M; Fan Y; Sarode A; et al. Correlating the Structure and Gene Silencing Activity of Oligonucleotide-Loaded Lipid Nanoparticles Using Small-Angle X-ray Scattering. ACS Nano 2023, 17, 11454–11465. [PubMed: 37279108]

(39). Brader ML; Williams SJ; Banks JM; et al. Encapsulation state of messenger RNA inside lipid nanoparticles. Biophys. J 2021, 120, 2766–2770. [PubMed: 33773963]

(40). Kloczewiak M; Banks JM; Jin L; et al. A Biopharmaceutical Perspective on Higher-Order Structure and Thermal Stability of mRNA Vaccines. Mol. Pharmaceutics 2022, 19, 2022–2031.

(41). Li S; Hu Y; Li A; Lin J; Hsieh K; Schneiderman Z; Zhang P; Zhu Y; Qiu C; Kokkoli E; et al. Payload distribution and capacity of mRNA lipid nanoparticles. Nat. Commun 2022, 13, 5561. [PubMed: 36151112]

(42). Fan Y; Yen C-W; Lin H-C; et al. Automated high-throughput preparation and characterization of oligonucleotide-loaded lipid nanoparticles. Int. J. Pharm 2021, 599, 120392. [PubMed: 33639228]

(43). Cui L; Pereira S; Sonzini S; et al. Development of a high-throughput platform for screening lipid nanoparticles for mRNA delivery. Nanoscale 2022, 14, 1480–1491. [PubMed: 35024714]

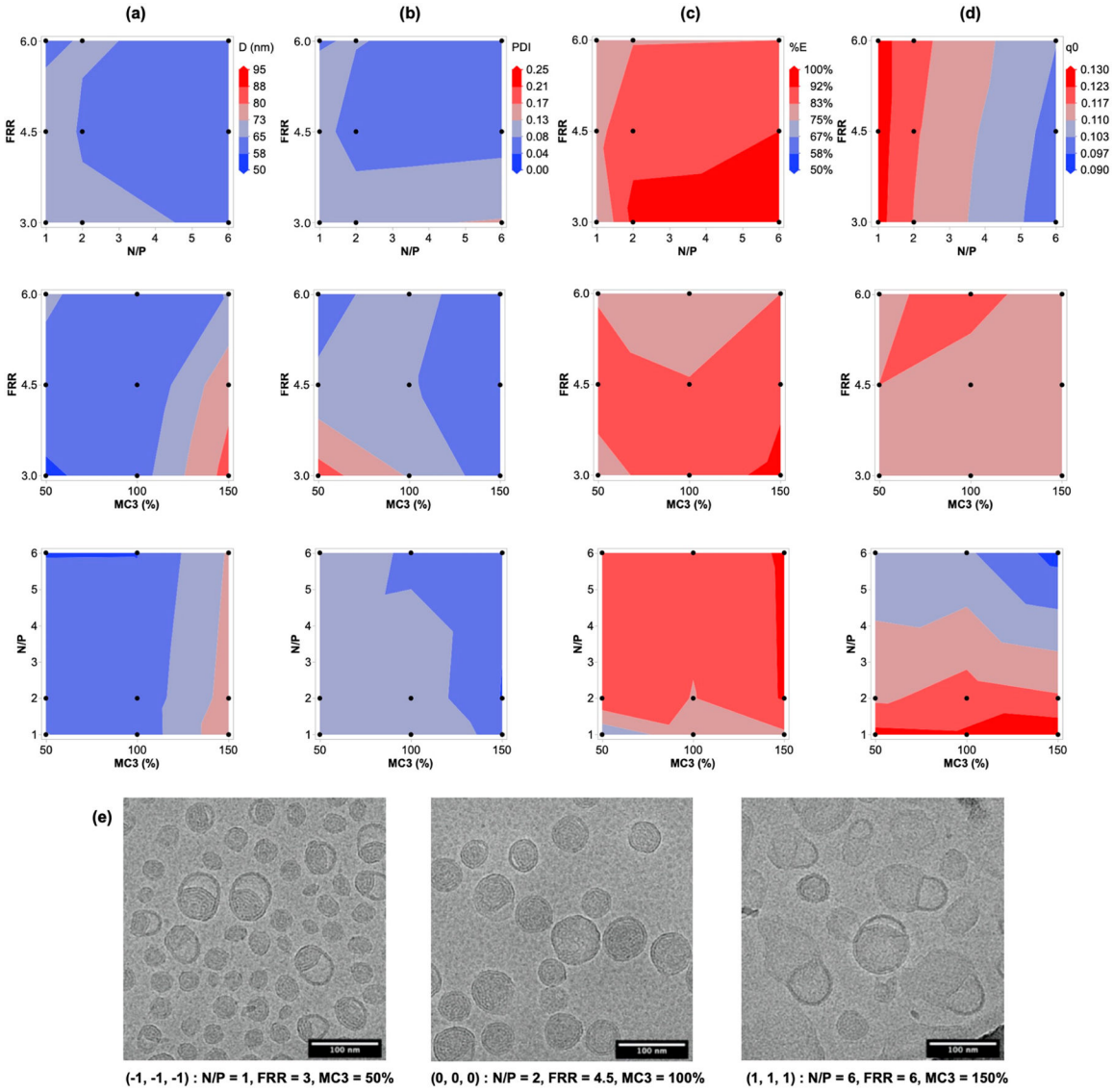

Figure 1.

DOE data for ASO-LNPs generated with a coaxial turbulent jet mixer. Surface plots are shown for each combination of the three investigated factors for (a) particle size (*D*, nm), (b) particle size distribution (PDI), (c) % encapsulation (%E), and (d) q_0 peak position ($Å^{-1}$) as measured by SAXS. Measured conditions are shown as black dots for reference. (e) CryoEM images are shown for samples from the low, center, and high conditions of the design space.

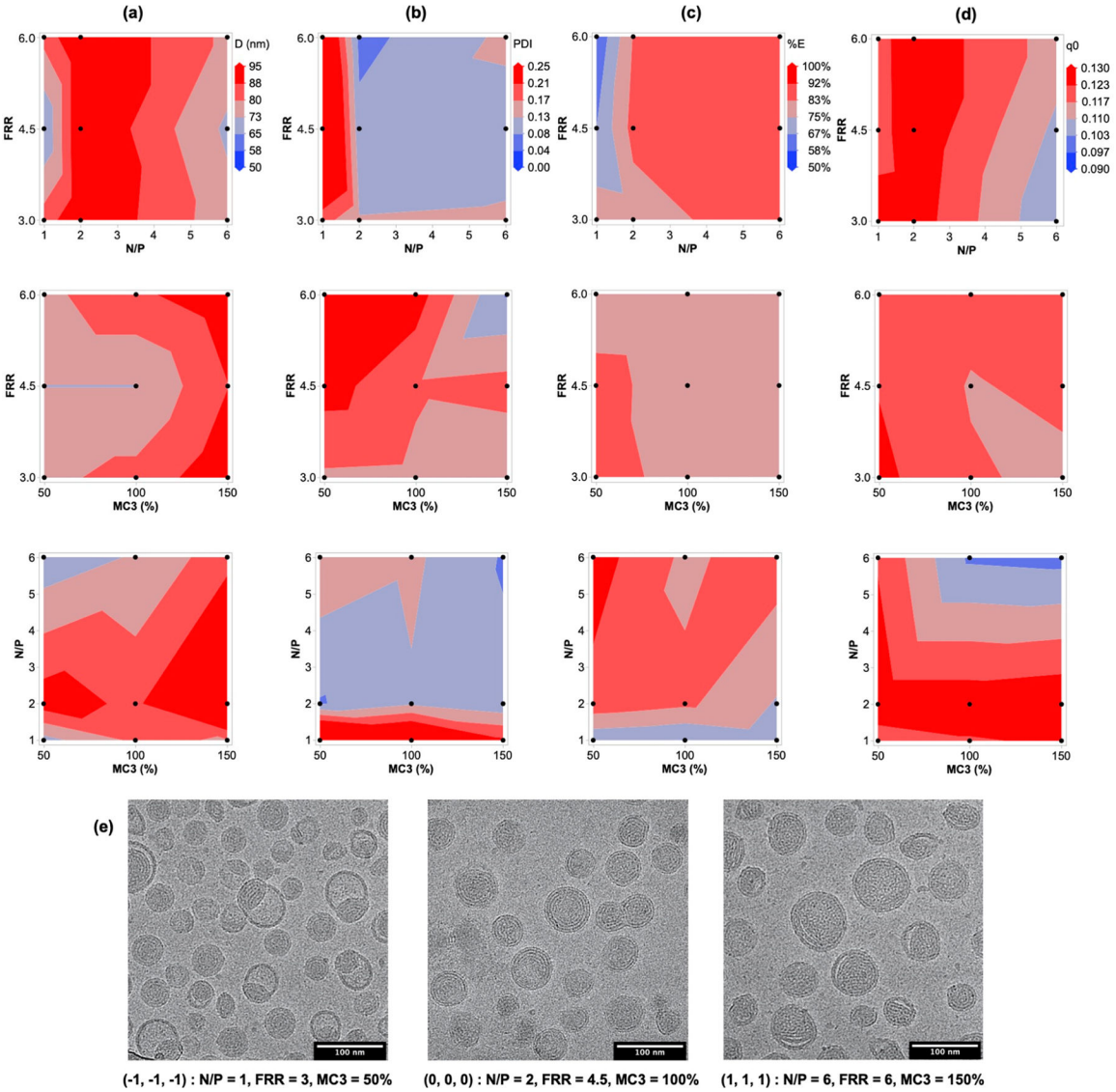

Figure 2.

DOE data for ASO-LNPs generated with a microfluidic mixer. Surface plots are shown for each combination of the three investigated factors for (a) particle size (*D*, nm), (b) particle size distribution (PDI), (c) % encapsulation (%E), and (d) q_0 peak position ($Å^{-1}$) as measured by SAXS. Measured conditions are shown as black dots for reference. (e) CryoEM images are shown for representative samples from the low, center, and high conditions of the design space.

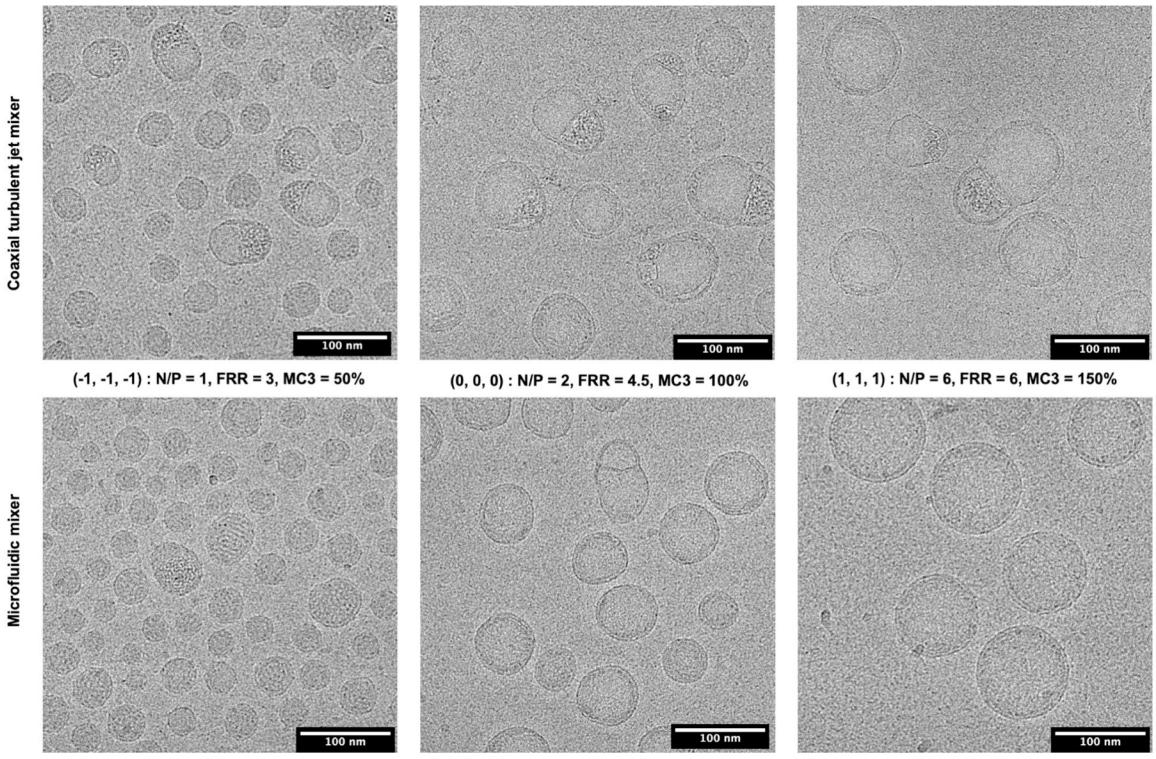

Figure 3.

mRNA-LNPs produced with a coaxial turbulent jet (top) or microfluidic mixer (bottom). CryoEM images are shown for representative samples after dilution and concentration. Sample conditions shown are low (−1, −1, −1), center (0, 0, 0), and high (1, 1, 1).

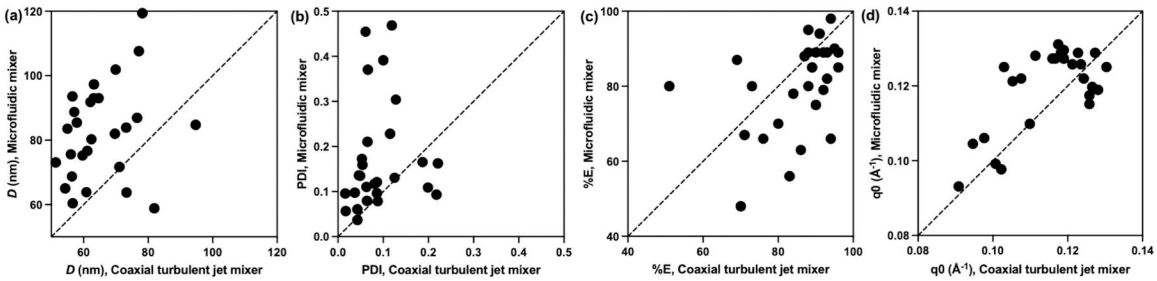

Figure 4.

ASO-LNP data for matched preparation conditions were plotted for the microfluidic mixer versus the coaxial turbulent jet mixer. Data were plotted for (a) particle size (D, nm), (b) particle size distribution (PDI), (c) percentage of encapsulated ASO (%E), and (d) q_0 peak position ($Å^{-1}$) as measured by SAXS. The dashed line is used to show what data would look like if there were direct correlation between mixers.

Table 1.

Full-Factorial ASO-LNP DOE Design

factor	no. of levels	low (−1)	center (0)	high (1)
Flow rate ratio (FRR)	3	3:1	4.5:1	6.0:1
N/P ratio	3	1	2	6
MC3 content (relative to Onpattro formulation, on molar basis)	3	50%	100%	150%